Photoemission investigation of polycrystalline and amorphous tellurium*

R. A. Powell and W. E. Spicer
Stanford Electronics Laboratories, Stanford University, Stanford, California 94305
(Received 23 October 1973)

Photoemission measurements of amorphous and polycrystalline Te films have been made in the photon energy range 4.8–11.6 eV in an ultrahigh vacuum of pressures less than 10^{-10} Torr. In contrast with the group-IV semiconductors Ge and Si, the photoemission spectra for both ordered and disordered films is remarkably similar with two broad peaks in the valence-band density of states located 1.7 and 4.6 eV below the top of the valence band. In addition, direct transitions do not appear to be very important in determining the photoemission spectra of either the amorphous or polycrystalline films. Differences in the density of states are second order and are brought out by measuring the second derivative of the photoemission spectra. Valence-band structure for the polycrystalline films lying within about 0.5 eV of the band edge is lost in the amorphous phase; however, weak conduction-band structure located 5.4 eV above the top of the valence band is observed in both films. Higher lying conduction-band structure appears to be smeared out in the amorphous films. The absolute photoelectric yield was measured and no evidence for density of states tailing below the *d*-like second conduction band, such as reported by Laude *et al.*, was found in either amorphous or polycrystalline films. The separation of the upper two peaks in the valence-band density of states is in good agreement with a molecular-orbital calculation which we present for trigonal Te; however, the calculated valence-band width is much too small by about 7.5 eV.

I. INTRODUCTION

Over the past several years, the photoemission technique has been used to investigate a variety of materials that exhibit both an amorphous and a crystalline phase (e.g., elemental Ge,[1] Si[2]), the Ge_xTe_{1-x} binary system,[3] and the chalcogenide glasses As_2S_3 and As_2Se_3.[4] Along with other measurements such as optical absorption and reflectivity, these studies have led to an increased understanding of the effect of short- and long-range order on the electronic structure of these materials. In this paper we present recent ultraviolet (uv) photoemission studies of amorphous and polycrystalline Te. For the amorphous case, these were the first such uv photoemission studies reported.[5] Te is particularly interesting to study because of its peculiar, highly anisotropic chain lattice.[6] Composed of long helical chains of atoms, one may regard Te as structurally closer to an organic polymer than to the more familiar group-IV semiconductors, Ge or Si. In the crystal, which is trigonal, these chains run parallel to one another along the *c* axis and are located at the center and corners of a regular hexagon. The bonding between Te atoms in the same chain is covalent, while the interaction between atoms in neighboring chains is partly van der Waals in nature and partly metallic and accounts for the long-range order of the crystalline phase. This long-range order is lost in the amorphous phase where, it is believed, the chains are broken up, distorted, and randomly oriented.[7] On the other hand, short-range order is retained in the amorphous solid with Te-Te bond lengths and bond angles not strongly different than for the trigonal crystal.[8] By studying the amorphous-to-crystalline transition in Te, then, one can conveniently examine the effect of long-range order on its electronic structure. It is worth noting that in this respect Te is much better suited than Se, with which it is often compared. Although both Te and Se have identical trigonal crystal structures, amorphous Se is believed to consist of a mixture of two structural species—helical chains and eight-membered puckered Se_8 rings.[6] For Se then, comparison of the disordered phase with the trigonal is complicated. For Te, no such rings have been detected in the amorphous phase, simplifying comparison with the crystalline form.

II. EXPERIMENTAL METHODS

The experiments reported here have been performed on amorphous and polycrystalline thin films of Te. The amorphous films were prepared by vapor deposition of high-purity Te (99.999%) onto a fused silica substrate held at 100 °K during evaporation. Te films prepared in this way are known from electrical and optical measurements of Keller and Stuke[9] to be amorphous. Fused silica was chosen as a substrate to avoid any substrate-induced ordering of the films; however, identical photoemission results were obtained using either polished heat-cleaned Mo or stainless steel substrates. During evaporation, the main chamber pressure was $(5-9)\times10^{-10}$ Torr. Subsequent photoemission measurements were made *in situ* at pressures less than 10^{-10} Torr with the substrate still held at 100 °K. Sample films were typically 1000 Å thick as measured with a quartz crystal thickness monitor. No difference in amor-

phous film properties were noted using deposition rates of 5 and 50 Å/sec. The polycrystalline films were formed in the several ways mentioned below and gave nearly identical photoemission spectra. In one case, the as-deposited amorphous films were slowly warmed from 100 °K to room temperature where subsequent photoemission measurements were made. Polycrystalline films were also prepared directly by vapor deposition of Te onto a substrate held at room temperature or at 150 °K. These films prepared by direct evaporation as well as those prepared by annealing the amorphous films to room temperature were determined to be polycrystalline by x-ray diffractometer measurements. Based on the widths of peaks in the x-ray data, we estimate that the average crystallite size for these films is on the order of 650 Å. The energy distributions of the photoemitted electrons (EDC's) were measured using the ac-modulated retarding potential method of Spicer and Berglund[10] as improved by Eden.[11] In addition, third derivatives of the photocurrent, SEDC's, which are proportional to the second derivative of the EDC's, were directly measured by sychronously detecting the third harmonic of the ac-modulation applied to the retarding ramp voltage. The technique of using higher derivatives of the EDC's in photoemission is discussed in Refs. 12–15. In the present work, we have used the SEDC to provide a better display of subtle features found in the EDC (e.g., shoulders or weak peaks riding on a smooth background curve). Such structure existing in the EDC is greatly accentuated in the SEDC and therefore easier to locate in energy. Photons in the range 3–12 eV were supplied by a Hinteregger-type H_2 discharge lamp and a McPherson monochromator (Model No. 225). The upper limit of $\hbar\omega = 12$ eV was set by the transmission cutoff of the LiF window that seals off the ultrahigh-vacuum chamber from the monochromator.

III. BAND-STRUCTURE CALCULATION FOR TRIGONAL Te

Before presenting the experimental results, we consider the electronic structure of trigonal Te. It is hoped that this will provide the reader with a general framework in which to view the photoemission data. Over the last few years, several calculations have been published for the trigonal crystal.[16–21] We present the results of one such calculation in Fig. 1. Done by Treusch and Sandrock[19] using a group-theoretical treatment based on the Kohn-Rostoker method,[22] this band structure preserves the salient features of the other calculations. Assuming no mixing of the atomic states, one expects Te to exhibit a triplet of p bands derived from the atomic $5s^2 5p^4$ configuration. The two lower triplets (generally referred to as p_1 and p_2) are occupied by electrons and determine the upper valence bands.[16] The upper triplet (referred to as p_3) is unoccupied by electrons and determines the lowest conduction band. This is seen to be the case in Fig. 1 where the top of the p_2 band sets the valence-band maximum (taken as the zero of energy) and the bottom of the p_3 band at H sets the band gap of 0.33 eV. In addition, because the trigonal chain lattice contains three atoms per unit cell, each of these bands is itself seen to be a triplet of subbands, where the subband splitting is seen to be about 0.1 eV. A further peculiar feature of the band structure is the energy gap which exists between the p_1 and p_2 groups of valence

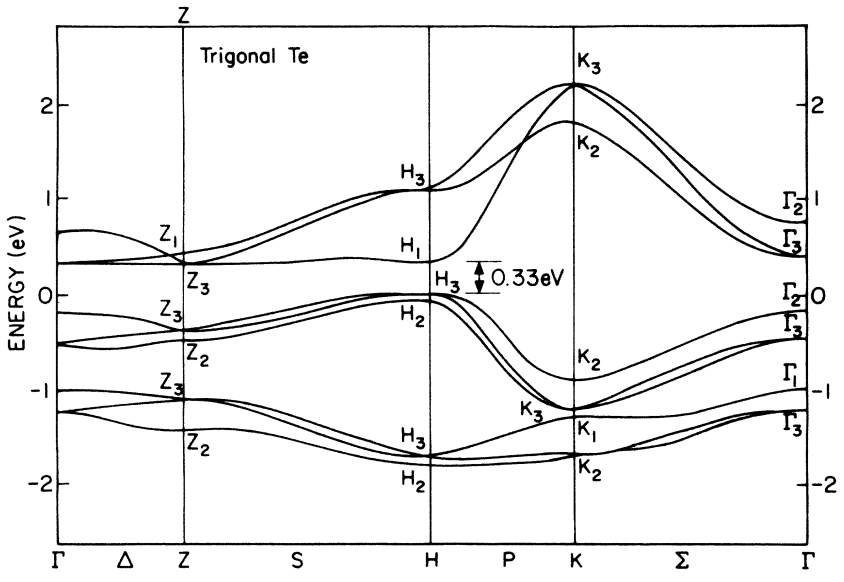

FIG. 1. Band structure of trigonal Te calculated by Treusch and Sandrock (Ref. 19) using the Kohn-Rostoker method (Ref. 22).

bands. This feature will be discussed later (Sec. IV) in connection with the shape of the reflectivity spectrum. Although the calculation shown in Fig. 1 gives a qualitative picture for the band structure of trigonal Te, one must be careful in using the absolute energy values shown. For example, the calculated width of the $5p$ valence bands (seen in Fig. 1 to be about 2 eV) is considerably smaller than the value of about 7 eV that is in fact found experimentally.[23]

Although not shown in Fig. 1, a second d-like conduction band (SCB) is found about 5 eV above the top of the valence band. A calculation by Maschke[21] indicates that this SCB is separated from the first p-like conduction band by an energy gap of about 2 eV. Also not shown in Fig. 1 are the valence states associated with the $5s$ electrons and the $4d$ core states. These have been experimentally found to lie about 11.5 and 40.5 eV, respectively, below the valence-band maximum (VBM).[23] Of particular significance in understanding the amorphous-to-crystalline transition in Te is the fact that the first direct gap ($\Delta E = 0.33$ eV) is not located at the center of the Brillouin zone near Γ. Instead it is located at the edge of the Brillouin zone, in the neighborhood of the H point, a direction from Γ corresponding to a crystallographic axis neither parallel nor perpendicular to the c axis. Now, the band structure in the direction H-K is thought to be largely determined by the interaction *between* chains of Te atoms,[24] whereas throughout the rest of the Brillouin zone the over-all appearance of p_1, p_2, and p_3 is determined by the short-range chemical bonding *within* the chains. Going over to the amorphous phase, we would then expect states in the neighborhood of H to be most sensitive to the loss of long-range order. In this way, one may roughly separate out the contributions of long- and short-range order to the electronic band structure of Te. Unfortunately, because of the relative flatness displayed by the bands in Te (see Fig. 1), it has been rather difficult to assign structure, observed in the optical spectra (e.g., ϵ_2, reflectivity, and absorption), to specific regions of $\vec{k}$ space.[25,26] Such assignments are further complicated for Te where calculations indicate that optical structure is caused as much by rapid variations in interband oscillator strength as by critical points in the joint density of states.[27]

IV. REFLECTIVITY

In Fig. 2 we present the near normal incidence uv reflectivity spectrum for a polycrystalline film of Te formed by vapor deposition onto a fused silica substrate held at room temperature. These measurements were made *in situ* at pressures less than 10^{-10} Torr using the ultrahigh-vacuum reflectometer described by Endriz and Spicer.[28] Unfortunately, the reflectometer design does not allow the substrate to be held at low temperature so that the reflectivity for an amorphous Te film could not be measured. For comparison we also show in Fig. 2 the reflectivity spectrum for the trigonal single crystal made using light polarized parallel ($\vec{E} \parallel \vec{c}$) and perpendicular ($\vec{E} \perp \vec{c}$) to the c axis. The trigonal reflectivity shown is actually a composite of measurements by Stuke and Keller[29] for $\hbar\omega < 5$ eV and by Cardona[30] for $\hbar\omega > 5$ eV. One notes that the reflectivity for the polycrystalline sample rather closely follows the average of the reflectivities for the trigonal crystal with $\vec{E} \perp \vec{c}$ and $\vec{E} \parallel \vec{c}$. This observation argues in favor of the sample having a polycrystalline structure. As mentioned earlier in Sec. II, similarly prepared Te films displayed a polycrystalline x-ray diffraction pattern. Both our data and the comparison data for the trigonal single crystal show that the reflectivity of Te is divided into two broad sections about a minimum near 6 eV. It has been suggested[30] that this peculiar feature in the optical spectrum can be understood by noting that the two groups of valence bands, p_1, and p_2, are separated by an energy gap (see Fig. 1). The joint density of states for transitions from p_1 and p_2 to the conduction band would then be low in the vicinity of the gap and give rise to a dip in the optical spectra.

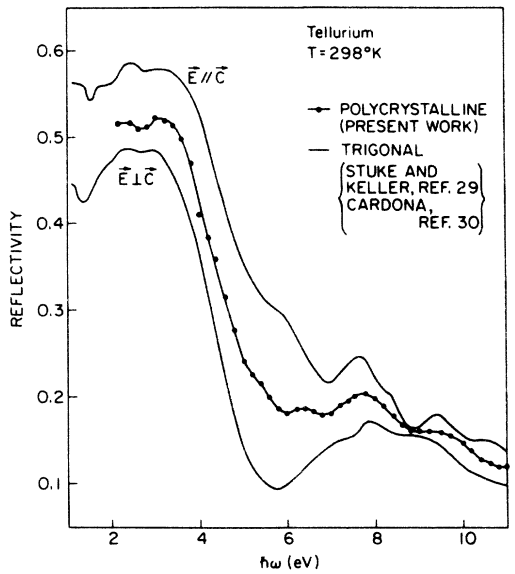

FIG. 2. Reflectivity spectrum for a polycrystalline Te film deposited at room temperature. For comparison, we show the reflectivity of trigonal Te measured at room temperature for light polarized with the electric field perpendicular ($\vec{E} \perp \vec{c}$) and parallel ($\vec{E} \parallel \vec{c}$) to the c axis. The data for $\hbar\omega < 5$ eV is from Stuke and Keller (Ref. 29) and for $\hbar\omega > 5$ eV from Cardona (Ref. 30).

Based on the EDC's to be presented for the polycrystalline film (Fig. 4) we detect a density-of-states minimum about 2.6 eV below the VBM. For photon energies in the neighborhood of the reflectivity minimum, i.e., $\hbar\omega = 5-7$ eV, the final states accessible from the minimum at -2.6 eV lie 2.4–4.4 eV above the VBM. Based on a recent calculation by Maschke,[21] the conduction-band density of states (CBDOS) for Te is vanishingly small in this region, between the top of the p_3 conduction band and the bottom of the d-like SCB. If this is indeed the case, one should attribute the peculiar shape of the Te reflectivity as much to a gap in the CBDOS as to the $p_1 - p_2$ gap in the valence-band density of states (VBDOS). That is, the pronounced dip in the reflectivity near 6 eV probably results because a large percentage of the allowed transitions near this photon energy have both small initial- *and* final-state densities.

V. PHOTOEMISSION STUDY OF AMORPHOUS AND POLYCRYSTALLINE Te

A. EDC's

In Figs. 3 and 4 we present selected EDC's for the photoemitted electrons from amorphous and polycrystalline Te. All the EDC's have been normalized to the quantum yield (which will be presented later as Figs. 8 and 9). That is, the area under an EDC equals the measured yield at that photon energy. In addition, the EDC's have been plotted so that the abscissa gives the *initial*-state energy of the photoemitted electrons. Initial-state electron energies are stated relative to the VBM and the energy scale has an instrumental uncertainty of ± 0.2 eV.

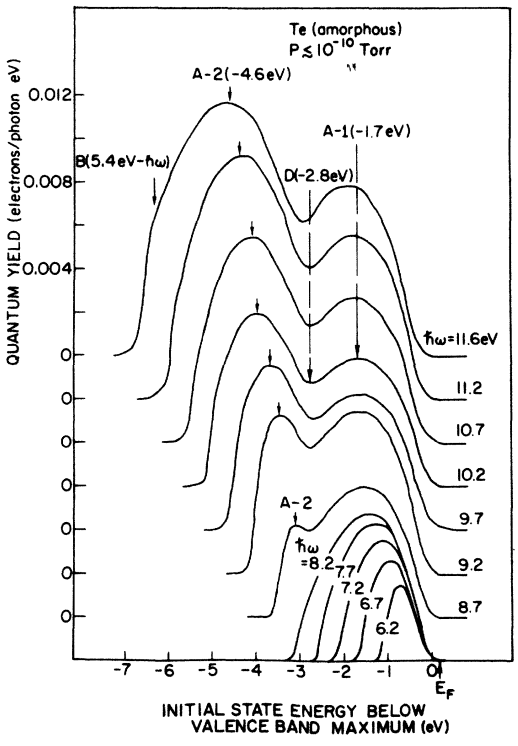

FIG. 3. Normalized energy distributions of the photoemitted electrons (measured at 100 °K) for amorphous Te films; $6.2 \leq \hbar\omega \leq 11.6$ eV.

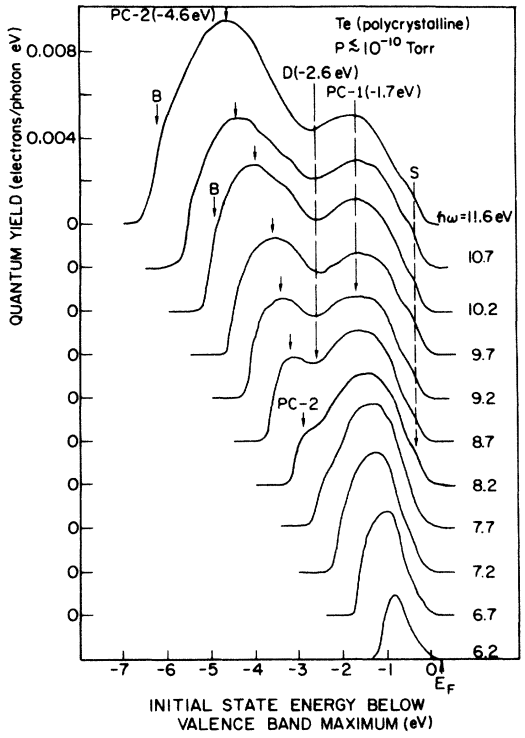

FIG. 4. Normalized energy distributions of the photoemitted electrons (measured at room temperature) for polycrystalline Te films; $6.2 \leq \hbar\omega \leq 11.6$ eV.

For both amorphous and polycrystalline films, the threshold voltage for photoemission (obtained from the zero intercept of the EDC's) is found to be 4.9 ± 0.1 eV. That is, photon energies in excess of 4.9 eV are needed to photoemit an electron from the sample into vacuum. In addition the work function of the copper-coated hemispherical collector can could be found by examining EDC's taken from the can's copper-coated back shutter (see Ref. 31 for a discussion of this technique). Based on these EDC's, the collector work function was found to be 5.0 ± 0.1 eV. Using this information, the Fermi level for both amorphous and polycrystalline Te samples was placed 0.15 ± 0.1 eV above the VBM, near the middle of the 0.33-eV forbidden gap.

The EDC's for the amorphous phase, shown in

Fig. 3, are relatively featureless. As the photon energy is increased above the threshold, the first prominent feature to appear in the EDC's is the peak labeled A-1. (Structure found in the photoemission data for amorphous or polycrystalline Te films will be denoted by the letter prefix A or PC, respectively.) Because of the effect of the threshold escape function on the distribution of electrons in the trailing edge of the EDC, both the shape and location of A-1 change as $\hbar\omega$ is increased above threshold. However, it is apparent that A-1 remains nearly stationary at -1.7 eV once the photon energy is sufficiently above threshold ($\hbar\omega \gtrsim 9.2$ eV). We therefore associate the peak A-1 with valence band structure located 1.7 ± 0.2 eV below the VBM. A second peak A-2 begins to appear in the EDC's for $\hbar\omega \gtrsim 8.2$ eV. On the basis of the EDC's shown in Fig. 3 one cannot be sure of the location of A-2, i.e., whether the peak has stopped moving out from under the threshold function by $\hbar\omega = 11.6$ eV where it appears peaked 4.6 eV below the VBM. In order to determine the location of A-2, the measurements were extended beyond the 12-eV cutoff imposed by the LiF window that seals the main chamber. Using a knock-off LiF window of the type developed by Krolokowski,[32] the LiF window could be knocked off exposing the sample to the low vacuum of the monochromator ($\simeq 10^{-4}$ Torr). There is then no window between the light source and sample so that photon energies greater than 12 eV can be used. Based on the EDC's taken for $12 < \hbar\omega < 15$ eV, the location of A-2 was found to remain stationary at -4.6 eV. We therefore assign A-2 to a maximum in the VBDOS located 4.6 ± 0.2 eV below the VBM.

It is interesting to note that the minimum D between A-1 and A-2 is fixed at -2.8 eV for all $\hbar\omega$ for which it appears. Also, a slight break B appears in the slope of the trailing edge of the EDC's that corresponds to conduction band structure 5.4 eV above the VBM. This feature is brought out more clearly in the SEDC's to be presented later, where it appears as structures A-6 and PC-6.

Although in the simple analysis one may extract information from the EDC's in terms of the existence and location of structure, the shape of the photoemission spectra can also be important. For example, it has been possible to argue against a $\vec{k}$-conserving model for amorphous Ge on the grounds that the model did not reproduce the *shape* of the leading edges observed in the EDC's.[33] For Te where, as we will see, the location of major structure in the EDC's is quite similar for both ordered and disordered films, the shape of the EDC's is also important. In this respect, note that for low photon energies, $\hbar\omega \lesssim 7.2$ eV, the EDC's for the amorphous films (Fig. 3) are quite symmetric about the peak A-1 and that the leading edges superimpose nicely. On the other hand, in Fig. 4 where the EDC's for the polycrystalline films are presented, no such symmetry is observed for $\hbar\omega \lesssim 7.2$ eV.

There are other differences as well. A shoulder S appears in the leading edge of the polycrystalline EDC's for $\hbar\omega \gtrsim 7.7$ eV that is notably absent in the amorphous EDC's. This shoulder is seen to extend about 0.5 eV down from the VBM. However, the trailing edge of the EDC's displays the same break B in slope that was seen in the EDC's for the amorphous films. Again this feature appears to correspond to conduction band structure located about 5.4 eV above the VBM. As for the amorphous case, the EDC's for the polycrystalline films are dominated by two broad peaks, labeled PC-1 and PC-2. PC-1 remains stationary at -1.7 eV once photon energy is sufficiently above threshold ($\hbar\omega \gtrsim 9.2$ eV). We assign PC-1 to a maximum in the VBDOS located 1.7 ± 0.2 eV below the VBM. As was the case for A-2 in the amorphous films, it is not clear whether PC-2 has stopped moving out from under the threshold function by $\hbar\omega = 11.6$ eV. It can be seen, however, by comparing Figs. 3 and 4 that for all photon energies the location of PC-2 and A-2 is identical. Based on higher-energy EDC's, A-2 was located at -4.6 eV. We likewise assign PC-2 as a maximum in the VBDOS located 4.6 ± 0.2 eV below the VBM. This assignment is in agreement with recent x-ray photoemission data.[23,34] Although the location of peaks PC-1 and PC-2 correspond to A-1 and A-2 of the amorphous phase, respectively, the EDC's for the polycrystalline films display considerably more fine structure about the two peaks. The EDC's for the amorphous case are smoothed by comparison. The origin of this fine structure is brought out more clearly in the SEDC's (to be presented as Fig. 5). We note that the minimum D that appears between PC-1 and PC-2 is shifted up in energy some 0.2 eV, compared with its location in the amorphous EDC's.

B. SEDC's

For each EDC shown in Figs. 3 and 4, the SEDC (proportional to the second derivative of the EDC) has also been measured. We present in Fig. 5 a comparison of SEDC's for the amorphous and polycrystalline films at selected photon energies $\hbar\omega = 6.7$, 7.7, and 9.7 eV. For convenience, the corresponding EDC's at these photon energies, which were discussed in Sec. V. A, are compared in Fig. 6. The sign of the SEDC has been chosen so that regions of negative curvature (e.g., peaks and shoulders) in the EDC come out as peaks in the higher-derivative curve. We regard the use of

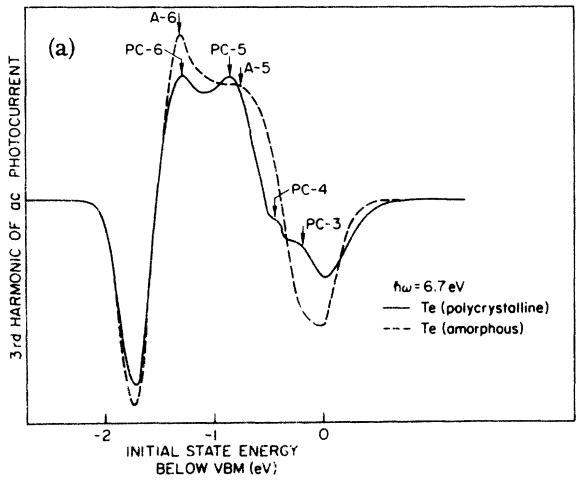

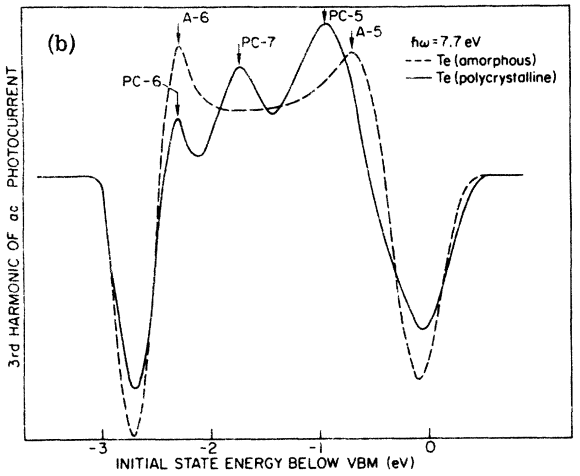

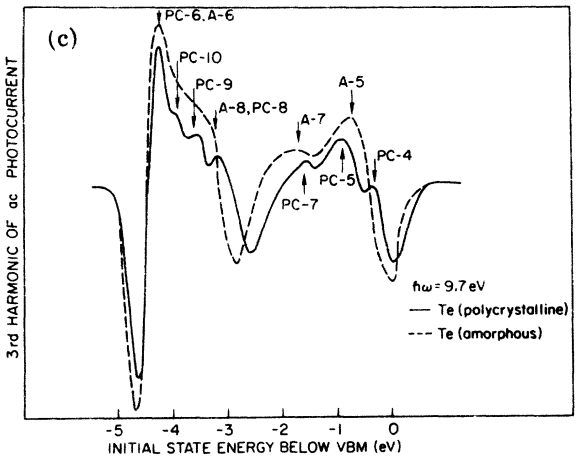

FIG. 5. Selected SEDC's for amorphous and polycrystalline Te films. $\hbar\omega = 6.7$, 7.7, and 9.7 eV. The sign of the SEDC was chosen so that regions of negative curvature (e.g., peaks and shoulders) in the EDC come out as peaks in the SEDC.

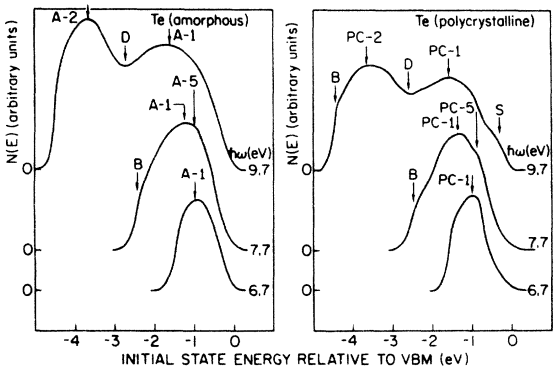

FIG. 6. Selected normalized EDC's for amorphous and polycrystalline Te films; $\hbar\omega = 6.7$, 7.7, and 9.7 eV.

the SEDC's as a means of accentuating fine structure observed in the EDC's. In this context, one must be careful of giving too much weight to structure observed in the SEDC's. For example, a structure that is relatively minor in the EDC's may show up as a pronounced peak in the SEDC's. This peak, however, would account for only a small fraction of the total oscillator strength represented by the EDC's.

For $\hbar\omega = 6.7$ eV two structures PC-3 and PC-4 appear in the polycrystalline SEDC that are totally lacking for the amorphous case. The initial state energy of PC-3 and PC-4 remains fixed in the SEDC's over a wide range of photon energies and suggests that these structures are associated with structure in the VBDOS located 0.2 and 0.4 eV, respectively, below the VBM. The structure PC-5 which, based on its fixed initial-state energy over a wide range of $\hbar\omega$, has been assigned to structure in the VBDOS 1.0 eV below the VBM, is shifted toward E_F for the amorphous SEDC's where it appears as A-5 located 0.7 eV below the VBM. This shift, which occurs in all the measured SEDC's, is clearly brought out in the SEDC for $\hbar\omega = 7.7$ eV (Fig. 5) and in the EDC's for $\hbar\omega = 7.7$ eV (Fig. 6), where PC-5 and A-5 appear as weak structures. In addition, for 7.7 eV, a new structure PC-7 is seen for the polycrystalline case that is notably absent in the amorphous SEDC at this photon energy. By $\hbar\omega = 9.7$ eV, the SEDC for both phases of Te has separated into two broad structured maxima (Fig. 5) reflecting the two broad VBDOS peaks observed in the EDC's at this photon energy (Fig. 6). We note in the SEDC for $\hbar\omega = 9.7$ eV that structure PC-4 is clearly absent in the amorphous case. Two other structures present in the polycrystalline case, PC-9 and PC-10, are probably both present in the amorphous SEDC but appear to be smeared out into a broad shoulder. Since their respective final-state energies remain constant with increas-

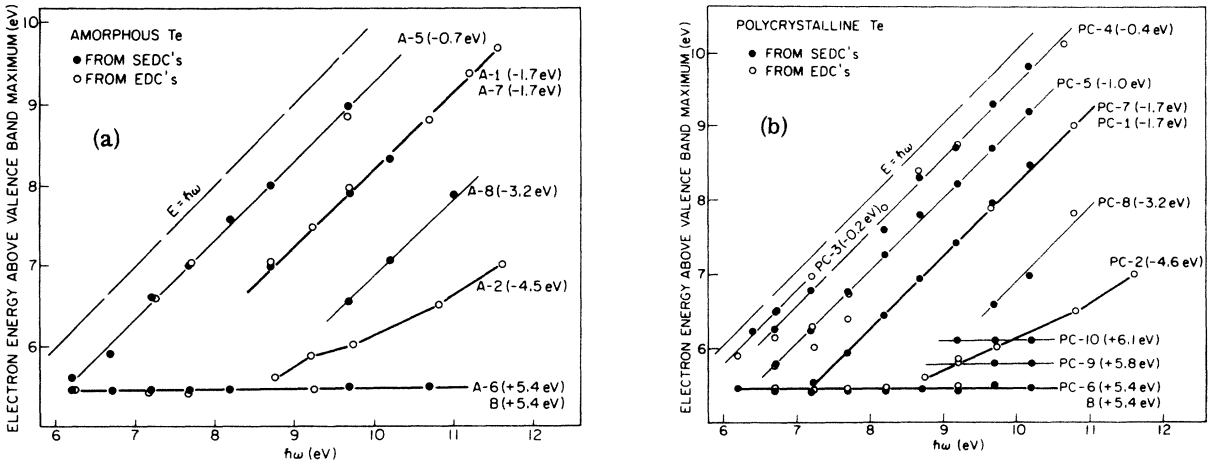

FIG. 7. Structure plots summarizing the structure observed in the EDC's and SEDC's for amorphous and polycrystalline Te films. The more prominent structures are indicated by a heavier line.

ing photon energy, these two structures have been associated with structure in the CBDOS at 5.8 and 6.1 eV. All the SEDC's shown in Fig. 5 display a pronounced peak for both amorphous (*A*-6) and polycrystalline (PC-6) films. This feature corresponds to CBDOS structure located 5.4 eV above the VBM. Some evidence for this structure is given by the break *B* in the EDC's of Figs. 3 and 4.

In Fig. 7 we have summarized all the structure observed in the EDC's and SEDC's for both amorphous and polycrystalline Te. In these plots, structure in the CBDOS plots horizontally (i.e., does not move with photon energy), while structure in the VBDOS moves with photon energy (i.e., $\Delta E = \hbar\omega$). The structure plot for the polycrystalline sample is in good agreement with similar features in the VBDOS and CBDOS of single-crystal trigonal Te, determined by uv photoemission in the range $5.2 \leq \hbar\omega \leq 9.0$ eV.[14]

C. Quantum yield

In Figs. 8 and 9 we present the spectral distributions of the quantum yield for $\hbar\omega < 12$ eV for both the polycrystalline and amorphous Te films. The sample reflectivity has not been taken into account so that yields are expressed as electrons per *incident* photon. Light intensities were measured using the absolute response of a calibrated Cs_3Sb phototube.[35] For comparison, the measured yield of Apker *et al.*[36] for similarly prepared polycrystalline Te films is shown. The agreement is quite good. Recent results of Ballantyne[37] were used to fit the energy dependence of the yield over a range of about 2 eV as seen in the insert in Fig. 9. The energy dependence of the yield Y, derived by Ballantyne for the case of a rectangular distribution of excited electrons, is $Y \propto (\hbar\omega - E_T)^3/(\hbar\omega)^2$, where $\hbar\omega$ is photon energy and E_T is the threshold. The extrapolated value for the photoemission threshold of Te is found to be about 5 eV in good agreement with the value obtained earlier from the zero in-

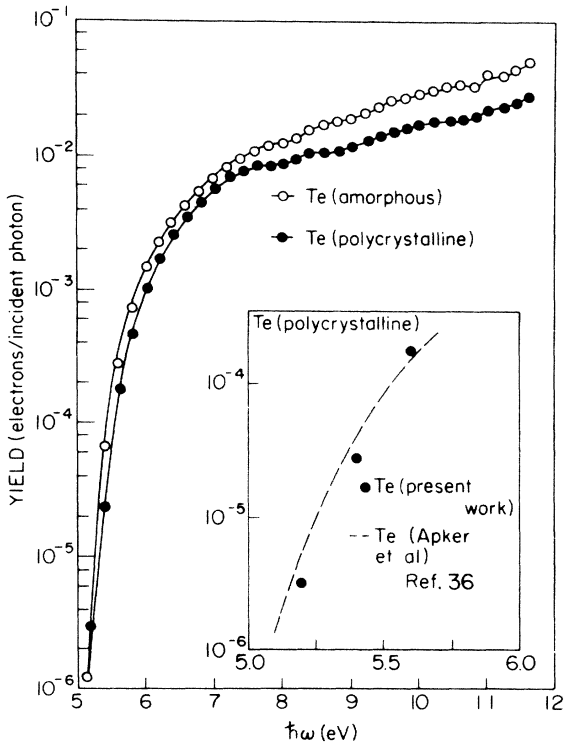

FIG. 8. Quantum yield ($5 \text{ eV} \leq \hbar\omega \leq 12$ eV) for amorphous and polycrystalline Te films. For comparison, the yield of similarly prepared polycrystalline films by Apker *et al.* (Ref. 36) is shown.

tercept of the EDC's. As might be expected, attempts to fit the energy dependence of the yield to a simple Fowler-type power law were not as successful near threshold.

As seen in Figs. 8 and 9, the quantum yields for both films rise from the photoemission threshold of about 5 eV and begin to level off about 2 eV higher. By $\hbar\omega = 11.6$ eV, the yields for the amorphous and polycrystalline films are of the order of 5×10^{-2} and 3×10^{-2} electrons per incident photon, respectively. At photon energies greater than about 6 eV, the yield of the amorphous film is seen to be consistently and significantly [(100–200)%] higher than that of the polycrystalline film. This large effect cannot be due to differences in the reflectivity of the film. Taking into account the reflectivity of the polycrystalline film (Fig. 2) would only raise its yield by about 20%. The observed differences in the yields may be qualitatively understood if one makes the reasonable assumption that lattice scattering is greater in the amorphous form of Te than in the trigonal crystal with long-range order. The amorphous film is then expected to have a higher yield since the increased probability of elastic or nearly elastic scattering will increase the probability of an excited electron reaching the escape cone.[38] This argument is admittedly tentative and presupposes that the electron-electron scattering length is larger than the defect scattering length. Were this not the case, the increased inelastic scattering expected for the amorphous film could significantly lower the number of electrons with sufficient energy to escape. The yield for the amorphous film might then be lower than that of the polycrystalline film in spite of the enhancement due to elastic scattering discussed above. The size of the trigonal crystallites present in the polycrystalline film is also expected to affect the total scattering and therefore the measured yield. For example, if the crystallites are small enough, the large number of internal surface barriers produced might actually increase the total scattering in the polycrystalline film above that of the amorphous film. This was in fact observed for Ge in which polycrystalline films containing small crystallites ($\ll 200$ Å) displayed a yield higher than that of the amorphous films which in turn had yields larger than that of polycrystalline films containing large crystallites.[31] The size of the crystallites in our polycrystalline films (about 650 Å) was sufficiently large so that this effect did not occur.

As can be seen in Figs. 8 and 9, the yield for both films is strictly monotonically increasing above the photoemission threshold. This contrasts a result obtained by Laude *et al.*[39] for Te films prepared in the same way as our polycrystalline films in which the yield exhibited nonmonotonic behavior below 5 eV. This behavior was taken as evidence for tailing of the CBDOS into the region below the *d*-like SCB. It was suggested that such DOS tailing was due to states associated with chain end imperfections produced in the evaporated film. In addition, the EDC's for these films displayed a tail on the trailing edge extending some 2 eV below the expected 5-eV threshold for photoemission. As can be seen in Figs. 3, 4, 8, and 9, we observe no such behavior in either the yield or the EDC's of similarly prepared evaporated Te films. The same was true for the amorphous Te films. We conclude from our results that tailing such as reported by Laude *et al.* is not a necessary feature of either amorphous or polycrystalline Te films.

VI. AMORPHOUS-TO-CRYSTALLINE TRANSITION IN Te

Based on structure observed in the EDC's and SEDC's (Figs. 3–7), the effect of reduced long-range order on the electronic DOS of Te appears to be the following: to first order, the DOS seem to be quite similar. However, certain features in the VBDOS and CBDOS are lost or smeared out, others merely shifted in energy, and still other features remain relatively unchanged. Specifically, valence band structure observed in the polycrystalline films that lies within about 0.5 eV of the VBM is lost in the amorphous films. That structural disorder in Te may severely affect those electronic states lying within about 0.5 eV of the band edge is supported by observations that the electrical gap of amorphous Te increases by about 0.5 eV over that in the crystal.[24] The corresponding change in the SEDC's for the amorphous films is the loss of structure observed at 0.2 and 0.4 eV below the VBM in the polycrystalline films (structures PC-3 and PC-4, respectively). Valence band structure lying somewhat deeper in energy is merely shifted up to higher energy in the amorphous phase. For example, PC-5, which appears at -1.0 eV in the polycrystalline SEDC's, is shifted up by about 0.3 eV in the amorphous case. The location of valence band structure sufficiently far from the VBM (e.g., PC-6 at -3.2 eV) appears to be unaffected by disorder. The pronounced peaks in the VBDOS located at -1.7 and -4.6 eV are retained in both phases. We associate these peaks with the p_1- and p_2-bands in the solid. As these states are primarily determined by the covalent bonding in the solid, i.e., the short-range order, the location of these maxima is not affected by the loss of long-range order. Although a weak structure in the CBDOS at 5.4 eV occurs for both phases, higher conduction band structure (PC-9 and PC-10 at 5.8 and 6.1 eV, respectively) appears to be smeared out in the amorphous phase. That the conduction band retains

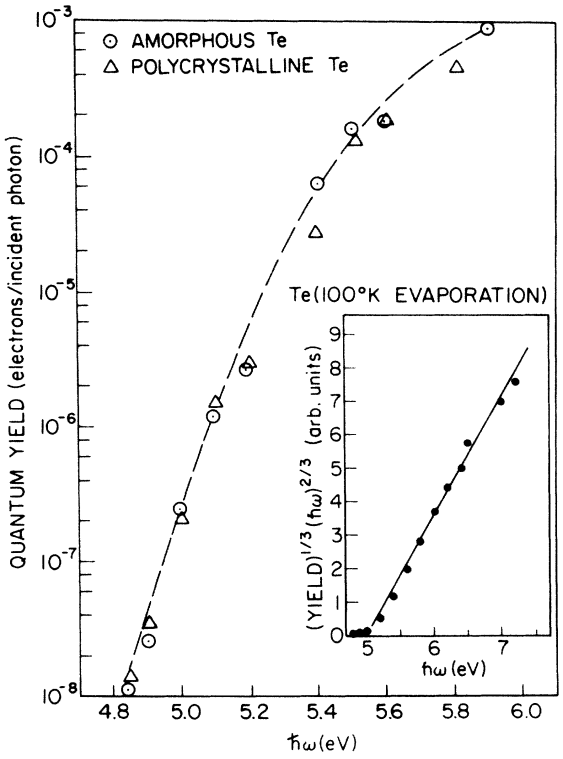

FIG. 9. Quantum yield ($\hbar\omega < 6$ eV) for amorphous and polycrystalline Te films. The insert shows that the yield data could be plotted as a straight line over a wide range of $\hbar\omega$ by using the relation due to Ballantyne (Ref. 37). In this plot, the photoemission threshold, determined from the $\hbar\omega$ intercept, is seen to be about 5 eV.

structure at 5.4 eV is unexpected, since in many amorphous semiconductors, all structure is lost in the higher-lying conduction band. It should be remembered, however, that this conduction band structure is relatively minor and is only brought out clearly in the SEDC's. In addition, the *d*-like nature of the SCB may render these states more atomic in nature than in other semiconductors and therefore less susceptible to disorder than one might expect.

As was pointed out in Sec. III, the relative flatness of the bands in Te suggest that most of the electronic transitions in Te are not well localized in $\vec{k}$ space. It is therefore difficult to assign the structures observed in the EDC's and SEDC's to particular regions of the Brillouin zone. This is possible, however, for PC-3 and PC-4 which are notably absent in the SEDC's for the amorphous phase. Since we expect states in the direction *H-K* to be most perturbed by the lack of long-range order, it is likely that the peaks at -0.2 and -0.4 eV are associated with initial states near the gap in the *H-K* region of the Brillouin zone. This argument has been presented previously by Laude *et al.* for similar structure observed in the VBDOS of single-crystal trigonal Te.[40]

As we discussed above, for Te the changes observed in the photoemission spectra are relatively minor. This sharply contrasts the case for semiconductors such as Ge, Si, and GeTe in which large first-order differences were observed between the EDC's for the amorphous and polycrystalline forms.[1-3] In interpreting the photoemission data for these materials it has been useful to consider both the effect of disorder on the VBDOS and CBDOS and the extent to which $\vec{k}$ conservation holds in the disordered phase. In Ge, for example, $\vec{k}$ conservation has been found to be unimportant in the amorphous form but very important in the crystalline form, and large differences between the CBDOS and VBDOS of amorphous and polycrystalline Ge films were observed.[1] Not surprisingly, the EDC's for polycrystalline Ge films are considerably different from those of amorphous films. For Te the situation is markedly different. In the first place, unlike Ge, there is little evidence for large effects due to direct transitions in the EDC's for the polycrystalline films (Fig. 4). Hence, one cannot determine from the EDC's whether $\vec{k}$ conservation is relaxed in the amorphous form of Te. Consequently, the amorphous-to-crystalline transition in Te displays none of the striking effects seen in the EDC's for Ge associated with the onset of direct transitions when long-range order was restored. In addition, the DOS for both amorphous and polycrystalline Te films is, to a first approximation, the same. That is, changes in the DOS are second order.

Besides the high-resolution uv photoemission studies reported here, there have been several other experiments to determine the effect of reduced long-range order on the DOS of Te.[34,41,42]

In one, the optical absorption from the spin-orbit split 4*d* core levels of amorphous and polycrystalline Te thin films was investigated by Sonntag *et al.*[42] in the range of photon energies 39–250 eV. Since the width of the 4*d* core states is small ($\lesssim 1$ eV) compared to the width of the conduction band, one expects the absorption from the 4*d* states to represent the CBDOS, provided the transition probabilities are independent of $\hbar\omega$ and that the one-electron approximation holds. Unfortunately, because of dipole selection rules that forbid transitions with $\Delta L = 0$, this method could not be used to directly observe the upper conduction band states in Te which are mainly *d* symmetric. These measurements show that the two main peaks of the lowest p_3 conduction band exist even in the disordered state of Te. These data also suggest that structure in the SCB may be smeared out in the amorphous phase. Based on theoretical calculations, one expects the lowest p_3 conduction band to

extend no more than about 3 eV above the VBM.[21] Since for the present study, the threshold for both amorphous and polycrystalline films was found to be well above this value (≃ 5 eV), we could not observe the p_3-conduction-band states to verify the above results. The results by Sonntag *et al.* for the SCB, however, are in qualitative agreement with the observed smearing out of structures PC-9 and PC-10 in the SEDC's for the amorphous phase.

A more direct investigation of the amorphous-to-crystalline transition in Te using a combination of uv and x-ray photoemission [electron spectroscopy for chemical analysis (ESCA)] has been presented recently by Shevchik *et al.*[34] Unfortunately, in this work it was not possible to determine the VBDOS of amorphous Te using uv photoemission because at the low substrate temperature (150 °K) used to prepare the amorphous film, a large oxygen peak appeard. This has been attributed to water vapor condensing on the film surface. No such problem was encountered in our work at even lower temperature (100 °K), probably because the chamber pressure during deposition ($< 10^{-9}$ Torr) was considerably lower than that of Shevchik *et al.* (5×10^{-6} Torr). Within the rather broad resolution of the ESCA experiment (≃ 1.5 eV) essentially no difference was seen between the VBDOS for dc-sputtered films of amorphous and polycrystalline Te. This negative result is not inconsistent with the changes observed in the present uv photoemission experiment, since the resolution obtained (≲ 0.2 eV) is almost an order of magnitude better. In like manner, ESCA studies of GeTe showed no differences between the amorphous and polycrystalline VBDOS.[43] Such differences were previously detected using the higher resolution afforded by the uv photoemission experiment.[3] On the other hand, the EDC's obtained for the amorphous and polycrystalline films (Figs. 3 and 4) are, to a first approximation, remarkably similar in that two peaks separated by about 3 eV at − 1.7 and − 4.6 eV dominate the VBDOS. The ESCA spectrum also consisted of two peaks at about 2.5 and 5.0 eV below the VBM. Although the location of the deeper maximum is in reasonable agreement with our value, the peak at − 2.5 eV is lower by about 0.8 eV.

In Fig. 10 we present the results of additional ESCA studies of crystalline Te by Pollak *et al.*[23] For comparison with the present work, an EDC for polycrystalline Te at $\hbar\omega = 11.6$ eV is shown. As seen in Fig. 10, the ESCA study locates two major peaks in the VBDOS separated by about 3 eV but lying 1.1 and 4.0 eV below the Fermi level. Depending on the extent of sample doping (i.e., on the position of the Fermi level relative to the VBM), these values may then be 0.6–0.9 eV higher than ours. This disagreement is not so great when one

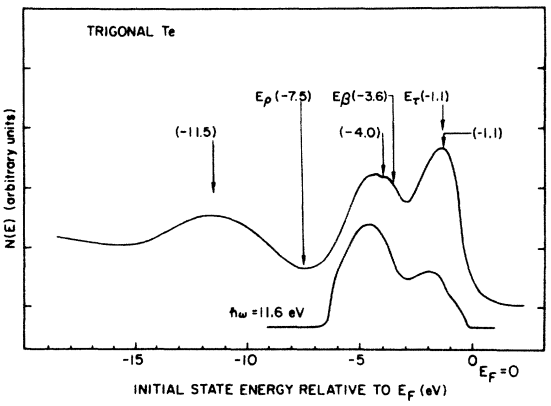

FIG. 10. VBDOS of trigonal Te determined using ESCA by Pollak *et al.* (Ref. 23). For comparison with the present work, an EDC from polycrystalline Te for $\hbar\omega = 11.6$ eV is shown. The energies of the β, ρ, and τ orbitals for trigonal Te determined by a molecular-orbital calculation are also shown. These values have been shifted up in energy so that E_τ coincides with the uppermost experimental peak at − 1.1 eV.

considers that the instrumental resolution for this ESCA measurement was about 0.5 eV. We note that the structure seen in the lower VBDOS peak near − 4.0 eV (see Fig. 10) was not observed in the present work.

It is also interesting to compare our results for the VBDOS of amorphous Te with theoretical treatments. There have been only two attempts made to calculate the DOS for amorphous Te, a molecular-orbital calculation by Hartmann and Mahanti[44] and a Green's-function calculation by Kramer.[45]

Hartmann and Mahanti have calculated the optical properties of random chains of Te atoms. Short-range order was preserved in the amorphous form by retaining a cluster of three atoms per unit cell as in the trigonal chain lattice. The one-electron wave function for a chain was then expressed as a linear combination of tight-binding wave functions for the three-atom cluster. Disorder was introduced by distorting bonds at the ends of the unit cells. Based on this model, a DOS spectrum was calculated for the amorphous phase. This DOS, however, bears little resemblance to the experimentally determined VBDOS in both the location and sharpness of structure in the p_1 and p_2 bands.

In the calculation by Kramer, local order was preserved in the amorphous phase by maintaining the same nearest-neighbor arrangement as in the trigonal crystal. Positional disorder was then simulated by a Gaussian broadening of the reciprocal lattice vectors in $\vec{k}$ space. By using the same pseudopotential form factors for the amorphous case as for the trigonal crystal, a DOS was calculated. Based on this calculation, bands near the

gap are broadened in the amorphous phase, particularly at points of high symmetry and all structure is lost in the d-like SCB. The over-all shape of the DOS associated with p_1, p_2, and p_3 remains. Except for the retention in the amorphous phase of structure in the CBDOS at 5.4 eV, these conclusions are qualitatively what was observed in the photoemission experiment. Quantitatively, however, the two pronounced peaks in the VBDOS associated with the p_2 and p_1 bands were calculated to lie about 1 and 3 eV below the VBM, respectively. The latter peak is therefore calculated to lie about 2 eV higher than is found experimentally. In addition, the d-like SCB is calculated to be about 1 eV too high. On the other hand, the width of the valence bands is too narrow by about a factor of 2. Experimentally, the $5p$ valence-band states in both amorphous and polycrystalline Te are found to extend some 7 eV below the VBM.[23,34] In Kramer's calculation, for both the crystalline and amorphous forms of Te, the valence-band width is only about 4 eV. It would be of great interest to see whether this calculation by Kramer can be used to generate EDC's for the amorphous phase that display features observed in the experimental curves. Unfortunately, band-structure calculations have seldom been used to generate photoemission spectra. Usually the spectrum of an optical constant, such as ϵ_2, is calculated and compared with experiment. However, as was stated earlier, in the case of Ge it was possible to argue against a $\vec{k}$-conserving model for the amorphous phase because calculations based on the model could not reproduce the measured photoemission spectra. Based on the present uv photoemission data for Te, one would require model calculations to generate EDC's for the amorphous and crystalline phases of Te that show little evidence of direct transitions and whose leading edges differ in shape for $\hbar\omega \lesssim 7.2$ eV (see Figs. 3 and 4 and Sec. V A).

VII. BONDING IN Te

As mentioned in the Introduction, the bonding in Te is covalent in the chains and partly van der Waals and partly metallic between the chains. The dissociation energy of bivalent Te_2 molecules, 2.3 eV, gives an idea of the bond strength within the chains. An attractive simplification in considering a system such as trigonal Te would be to ignore the between-chain interactions and treat the crystal instead as a one-dimensional molecular solid. Unfortunately, the bonding between chains, although weaker than the covalent bonding within the chains, is considerable and cannot be ignored. Thus, a one-dimensional model for Te is unrealistic. This is made plausible when one considers that a single Te atom is covalently bonded to only two nearest neighbors in the same chain, while it interacts with four next-nearest neighbors in adjacent chains each at a distance only about 20% larger than the nearest-neighbor separation. As for the view of Te as a molecular solid, one expects the absorption edge of a crystalline molecular solid to be determined by the molecules and their excited states and that this situation would only be slightly changed in the amorphous phase. For Te, however, the absorption edge is dramatically shifted by about 0.5 eV to higher energy in the amorphous phase.[24]

Any theory of the bonding in Te must account for the experimental facts. The short-range covalent bonding in the chains is experimentally represented by the two dominant peaks observed in the polycrystalline and amorphous EDC's (Figs. 3 and 4) at -1.7 and -4.6 eV. As mentioned earlier in Sec. VI, these peaks in the VBDOS have also been observed in separate ESCA experiments by Pollak *et al.*[23] and by Shevchik *et al.*[34] but at somewhat different initial state energies. The former workers have assigned peaks at -1.1 and -4.0 eV to the lone-pair band and bonding band, respectively, in support of a model for group-VI elements in twofold coordination discussed by Kastner.[46] Within this model, one tries to understand the band structure of Te by considering the four electrons that fill the $5p$ orbitals. Two of these electrons are unshared and form lone-pair bonds, while the remaining two electrons form bonds by pairing spins with the two-nearest-neighbor Te atoms. One expects that these bonding electrons will lie deeper in energy than the lone-pair electrons since they are repelled by the empty antibonding states. In this case then, the upper valence band of Te is formed by the lone-pair electrons. This contrasts the situation observed for the tetrahedral semiconductors such as Ge in which the valence band is formed by the bonding electrons and the conduction band by the antibonding electrons. One must be careful in using this model to interpret the experimental VBDOS for Te since it does not consider the two electrons per atom associated with the $5s$ levels and therefore does not consider the effect of sp hybridization. That atomic p orbitals cannot be a good representation for this system can be seen by noting that the bond angles for trigonal Te are 102.6° rather than 90° as in a cubic lattice. Unfortunately, since the coordination of the Te atoms does not belong to a tetrahedral lattice either, one cannot use the simplification of equivalent sp^3 orbitals when considering sp hybridization in Te. This problem has been treated in a recent molecular-orbital calculation by Chen,[47] who considered the effect of sp hybridization on the VBDOS of Se chains. In this calculation the $4s$ and $4p$ orbitals were assumed to hybridize into two equivalent bonding orbitals and two equivalent lone-

pair orbitals. Although, as might be expected, the lone-pair and bonding states contribute mostly to the upper and lower of the two peaks in the VBDOS, respectively, each state was found to contribute considerably [(30–50)%] to the strength of the other peak. The result of this calculation for Se suggests that one must be cautious of separating the two major peaks in the experimental VBDOS of trigonal Te into distinct lone-pair and bonding states as has been done previously.

In order to better understand the possible role of sp hybridization on the VBDOS of Te, we present a molecular-orbital calculation for the energy levels of the trigonal crystal. The approach used here is essentially the same one developed by Tutihasi and Chen[48] several years ago to treat trigonal Se. The 5s and 5p orbitals of the Te atom are assumed to hybridize into two equivalent sigma σ orbitals pointing along the Te-Te bond toward the two nearest neighbors in the chain, and two equivalent lone-pair orbitals. Linear combinations of the σ orbitals give bonding, α, and antibonding, β, orbitals, while the lone-pair orbitals combine to give orbitals ρ and τ that transform according to one of the irreducible representations of the trigonal symmetry group D_3. In this scheme, the σ orbitals contribute to the covalent bonding within the chains while the ρ and τ orbitals contribute to the bonding between chains. It is possible to express the energy of these orbitals in terms of the energies of the 5s and 5p atomic orbitals of Te by[48]

$$E_\rho = (1-2\gamma^2)E_s + 2\gamma^2 E_p \ , \quad E_\tau = E_p \ , \qquad (1)$$

$$E_\alpha = (E_\sigma - E_{\sigma\sigma'})/(1-S_\sigma) \ , \quad E_\beta = (E_\sigma + E_{\sigma\sigma'})/(1+S_\sigma) \ .$$

E_s and E_p are the energies of the 5s and 5p atomic orbitals, respectively, and $E_\sigma = \gamma^2 E_s + (1-\gamma^2)E_p$, where γ is related to the Te-Te bond angle θ (102.6°) through $\gamma^2 = [-\cos\theta/(1-\cos\theta)] = 0.17$. S_σ is the overlap integral between the two hybrid σ orbitals on nearest-neighbor Te atoms, and $E_{\sigma\sigma'}$ is the interaction energy between these σ orbitals.

Now in the solid the three orbitals ρ, β, and τ are filled and account for the six valence electrons per atom. The energy of the ρ and τ orbitals is easily calculated from Eq. (1) using the values $E_s = -18.4$ eV and $E_p = -8.55$ eV obtained from a free-atom relativistic Hartree-Fock-Slater calculation.[49] We find

$$E_\rho = -15.0 \text{ eV}, \quad E_\tau = -8.6 \text{ eV} \ . \qquad (2)$$

A considerable simplification in calculating the energy of the bonding orbital E_β can be achieved by first using the semiempirical formula due to Cusachs[50] to express $E_{\sigma\sigma'}$ as

$$E_{\sigma\sigma'} \simeq S_\sigma(2 - |S_\sigma|)E_\sigma \ . \qquad (3)$$

Substitution of Eq. (3) into Eq. (1) then gives

$$E_\beta/E_\sigma \simeq (1+2S_\sigma - S_\sigma^2)/(1+S_\sigma) \ . \qquad (4)$$

The factor on the right in Eq. (4) is relatively insensitive to the value of the overlap integral chosen. In fact, one finds that for values of S_σ in the range 0–1.0, $E_\beta/E_\sigma = 1.1$ to within 10%. We therefore approximate

$$E_\beta \simeq 1.1 \times E_\sigma = -11.3 \text{ eV} \ . \qquad (5)$$

In order to compare the calculated energies E_β, E_ρ, and E_τ [Eqs. (2) and (5)] with the experimental VBDOS, it is necessary to shift these values up in energy. This corresponds to the polarization energy of the solid which has not been included in the above molecular-orbital calculation.[51] In Fig. 10 we compare the VBDOS of trigonal Te measured by Pollak *et al.*[23] with the calculated energies of the three filled orbitals τ, β, and ρ. These energies have been shifted up so that τ coincides with the upper experimental VBDOS peak at -1.1 eV. The agreement of the upper two peaks is seen to be quite good; however, the calculated width of the valence band is about 7.5 eV too small. In addition, the calculation does not account for the broad ($\simeq$ 10 eV wide) maximum that appears at 11.5 eV below the Fermi level. This structure has been associated with the 5s core states in Te. The existence of such s bands in Te extending from about 10–14 eV below the VBM have been predicted by Maschke using a pseudopotential calculation.[21]

VIII. CONCLUSIONS

In conclusion then, high-resolution uv photoemission measurements have been used to study the amorphous-to-crystalline transition in Te and to determine important features in the d-like SCB and the p_1 and p_2 valence bands in both the amorphous and crystalline phase. For Te, in sharp contrast with the group-IV semiconductors Ge and Si, the EDC's of the amorphous and polycrystalline samples are remarkably similar. Differences in the DOS are second order and are brought out by using the presentation available in the SEDC's. In addition, direct transitions do not appear to be very important in determining the photoemission spectra of either the amorphous or polycrystalline films. For the crystalline material, this may be a consequence of the flatness of the valence bands.

The polycrystalline sample exhibits structure in the CBDOS at 5.4±0.2, 5.8±0.2, and 6.1±0.2 eV above the VBM. Two pronounced maxima in the VBDOS are located 1.7±0.2 and 4.6±0.2 eV below the VBM and have been associated with the p_1 and p_2 bands, respectively. Additional, weaker, valence band structure for the polycrystalline samples are located 0.2±0.2, 0.4±0.2, 1.0±0.2, and 3.2±0.2 eV below the VBM. We associate the structures 0.2 and 0.4 eV below the VBM with ini-

tial states in the direction H-K. The location of DOS structure for the polycrystalline sample is in good agreement with uv photoemission studies of single-crystal trigonal Te[14] and with results of x-ray photoemission crystalline and polycrystalline Te.[23,34]

For the amorphous sample, the CBDOS structure at 5.4 ± 0.2 eV is retained while higher conduction band structure appears to be smeared out. However, the two VBDOS maxima at -1.7 ± 0.2 and -4.6 ± 0.2 eV are retained. Additional valence band structure are located 0.7 ± 0.2 and 3.2 ± 0.2 eV below the VBM. Structure in the VBDOS within about 0.5 eV of the band edge is lost in going over to the amorphous form. The above features in the experimentally determined VBDOS for amorphous Te are in rather poor agreement with a molecular-orbital calculation of Hartman and Mahanti.[44] They are, however, in qualitative agreement with a recent Green's-function calculation by Kramer,[45] although in this calculation the valence-band width is some 3 eV too narrow.

No evidence for DOS tailing below the d-like SCB, such as reported by Laude *et al.*,[39] was observed in the yield, EDC's or SEDC's for either amorphous or polycrystalline films.

The location of the two pronounced peaks in the experimental VBDOS of Pollak *et al.*[23] for polycrystalline Te films are in reasonable agreement with a molecular-orbital calculation which we present for the trigonal crystal. However, the calculated valence-band width is too small by about 7.5 eV and does not predict the broad VBDOS maximum seen at 11.5 eV below the Fermi level.

---

*Work supported by the National Science Foundation through the Center for Material Science at Stanford University and the Advanced Projects Agency through the U. S. Army Research Office, Durham.

[1]T. M. Donovan and W. E. Spicer, Phys. Rev. Lett. 21, 1572 (1968).
[2]D. T. Pierce and W. E. Spicer, Phys. Rev. B 5, 3017 (1972).
[3]G. B. Fisher and W. E. Spicer, Proceedings of Fourth International Conference on Amorphous and Liquid Semiconductors, Ann Arbor, Mich., 1971 (unpublished); J. Non-Cryst. Solids 8-10, 978 (1972).
[4]P. Nielsen, Bull. Am. Phys. Soc. 17, 113 (1972).
[5]R. A. Powell and W. E. Spicer, Bull. Am. Phys. Soc. 18, 390 (1973).
[6]N. F. Mott and E. A. Davis, *Electronic Processes in Non-crystalline Materials* (Clarendon, Oxford, England, 1971).
[7]P. Grosse, *Springer Tracts in Modern Physics* (Springer, Berlin, 1969), Vol. 48.
[8]A. Axman, W. Gissler, A. Kollmar, and T. Springer, Discuss. Faraday Soc. 50, 74 (1970).
[9]H. Keller and J. Stuke, Phys. Status Solidi 8, 831 (1965).
[10]W. E. Spicer and C. N. Berglund, Rev. Sci. Instrum. 35, 1665 (1964).
[11]R. C. Eden, Rev. Sci. Instrum. 41, 252 (1970).
[12]L. W. James, R. C. Eden, J. L. Moll, and W. E. Spicer, Phys. Rev. 174, 909 (1968).
[13]N. V. Smith and M. M. Traum, Phys. Rev. Lett. 25, 1017 (1970).
[14]L. D. Laude, B. Fitton, and M. Anderegg, Phys. Rev. Lett. 26, 637 (1971).
[15]P. Nielsen, Bull. Am. Phys. Soc. 16, 349 (1971).
[16]J. R. Reitz, Phys. Rev. 105, 1233 (1967).
[17]D. J. Olechna and R. S. Knox, Phys. Rev. 140, A986 (1965).
[18]R. E. Beissner, Phys. Rev. 145, 479 (1966).
[19]J. Treusch and R. Sandrock, Phys. Status Solidi 16, 487 (1966).
[20]M. Hulin and M. Picard, Solid State Commun. 7, 1587 (1969).
[21]K. Maschke, Phys. Status Solidi 47, 511 (1971).
[22]W. Kohn and N. Rostoker, Phys. Rev. 94, 1111 (1954).
[23]R. A. Pollak, S. Kowalczyk, L. Ley, and D. A. Shirley, Phys. Rev. Lett. 29, 274 (1972).
[24]J. Stuke, J. Non-Cryst. Solids 4, 1 (1970).
[25]J. D. Haynes, E. T. Arakawa, and M. W. Williams, J. Appl. Phys. 39, 5527 (1968).
[26]S. Tutihusi, G. G. Roberts, R. C. Keezer, and R. E. Drews, Phys. Rev. 177, 1143 (1969).
[27]R. Sandrock, Phys. Rev. 169, 642 (1968).
[28]J. Endriz and W. E. Spicer, Phys. Rev. B 2, 1466 (1970).
[29]J. Stuke and H. Keller, Phys. Status Solidi 7, 189 (1964).
[30]The reflectivity data of M. Cardona are presented by J. Stuke, in *The Physics of Selenium and Tellurium* (Pergamon, New York, 1969), p. 3.
[31]C. G. Ribbing, D. T. Pierce, and W. E. Spicer, Phys. Rev. B 4, 4417 (1971).
[32]W. F. Krolokowski, Ph.D. dissertation (Stanford University, 1970 (unpublished).
[33]W. E. Spicer and T. M. Donovan, Phys. Rev. Lett. 24, 595 (1970).
[34]N. J. Shevchik, M. Cardona, and J. Tejeda, Phys. Rev. B 8, 2833 (1973).
[35]G. B. Fisher, W. E. Spicer, P. C. McKernan, V. F. Pereskok, and S. J. Wanner, Appl. Opt. 12, 799 (1973).
[36]L. Apker, R. Taft, and J. Dickey, Phys. Rev. 74, 1462 (1948).
[37]J. M. Ballantyne, Phys. Rev. B 6, 1436 (1972).
[38]R. N. Stuart and F. Wooten, Phys. Rev. 156, 364 (1967).
[39]L. D. Laude, R. F. Willis, and B. Fitton, Phys. Rev. Lett. 29, 472 (1972).
[40]L. D. Laude, B. Kramer, and K. Maschke, Phys. Rev. B 8, 5794 (1973).
[41]L. D. Laude and B. Fitton, J. Non-Cryst. Solids 8-10, 971 (1972).
[42]B. Sonntag, T. Tuomi, and G. Zimmerer, Phys. Status Solidi B 58, 101 (1973).
[43]N. J. Schevchik, J. Tejada, D. W. Langer, and M. Cardona, Phys. Rev. Lett. 30, 659 (1973).
[44]W. M. Hartmann and S. D. Mahanti, J. Non-Cryst. Solids 8-10, 633 (1972).
[45]B. Kramer, Festkörperprobleme XII, 133 (1972).
[46]M. Kastner, Phys. Rev. Lett. 28, 355 (1972).

[47]I. Chen, Phys. Rev. B 7, 3672 (1973).
[48]S. Tutihasi and I. Chen, Phys. Rev. 158, 623 (1967).
[49]T. A. Carlson, C. C. Lu, T. C. Tucker, C. W. Nestor, and F. B. Malik, Oak Ridge National Laboratory Report No. ORNL-4614, 1970 (unpublished).
[50]L. C. Cusachs, J. Chem. Phys. 43, S157 (1965).
[51]P. Nielsen, Phys. Rev. B 6, 3739 (1972).